LETTERS
PUBLISHED ONLINE: 3 JULY 2011 | DOI: 10.1038/NNANO.2011.97
nature nanotechnology

Electrically pumped waveguide lasing from ZnO nanowires

Sheng Chu[1†], Guoping Wang[1†], Weihang Zhou[2], Yuqing Lin[3], Leonid Chernyak[3], Jianze Zhao[1,4], Jieying Kong[1], Lin Li[1], Jingjian Ren[1] and Jianlin Liu[1*]

Ultraviolet semiconductor lasers are widely used for applications in photonics, information storage, biology and medical therapeutics. Although the performance of gallium nitride ultraviolet lasers has improved significantly over the past decade, demand for lower costs, higher powers and shorter wavelengths has motivated interest in zinc oxide (ZnO), which has a wide direct bandgap and a large exciton binding energy[1–6]. ZnO-based random lasing has been demonstrated with both optical and electrical pumping[7–10], but random lasers suffer from reduced output powers, unstable emission spectra and beam divergence. Here, we demonstrate electrically pumped Fabry–Perot type waveguide lasing from laser diodes that consist of Sb-doped p-type ZnO nanowires and n-type ZnO thin films. The diodes exhibit highly stable lasing at room temperature, and can be modelled with finite-difference time-domain methods.

Single-crystalline semiconductor nanowires have long been considered an excellent means by which to realize small and cost-effective Fabry–Perot (FP) type lasers, because of the optical feedbacks provided by the naturally formed flat facets in the ends of nanowires. Although optically pumped nanowire lasers have been reported widely[1–5], only a single cadmium sulphide (CdS) nanowire/silicon heterojunction laser has been demonstrated in an electrically driven configuration[11], and there is still a lack of high-efficiency homojunction lasers. When ZnO material is considered, this lack of efficient laser devices arises mainly because of the difficulty in achieving controllable p-type doping[12–14]. As the development of reliable p-type doping of ZnO progresses, more nanowire-based optoelectronic device will certainly emerge; for example, p-n homojunction nanowire light-emitting diodes (LEDs)[14] and photodiodes[15] have recently been realized. In this Letter, we report a homojunction diode that consists of p-type Sb-doped ZnO nanowires on a high-quality n-type ZnO film. Evident FP-type UV lasing was demonstrated, and the gain/feedback mechanisms and laser emission profile were studied in detail.

Figure 1 presents a schematic (Fig. 1a) and a photograph (Fig. 1b) of the device. Growth of the p-type ZnO nanowire/n-type ZnO film diode structure was carried out by means of a seed-assisted growth scheme[16,17]. A 1,050-nm-thick high-quality n-type ZnO seed film was grown on a *c*-plane sapphire substrate by plasma-assisted molecular beam epitaxy (MBE) (Supplementary Figs S1 and S2). Sb-doped p-type nanowires were then grown on top of the film by chemical vapour deposition (CVD). The *c*-axis of the ZnO nanowires perfectly follows the growth direction of the underlying film, resulting in a highly oriented vertical nanowire array (Fig. 1c, Supplementary Fig. S3). The length and diameter of the nanowires are, on average, 3.2 μm and 200 nm, respectively. Subsequent device fabrication details are given in the Methods.

The major merit of this device structure lies in the integration of the advantages of MBE and CVD. MBE results in the growth of high-quality thin films, but is not practical for the growth of nanowires because of its relatively low growth rate. CVD, on the other hand, results in the synthesis of high-quality nanowires with a fast growth speed, but cannot satisfactorily achieve the controllable growth of multi-segment nanowires with different conductivity types. Therefore the approach of growing p-type nanowires using CVD on high-quality n-type films grown by MBE can solve this dilemma and produce controllable p-n homojunctions. The single-crystalline nature of ZnO nanowires was confirmed by high-resolution transmission electron microscopy (TEM) imaging analysis (Supplementary Fig. S4). The incorporation of Sb dopant was demonstrated by X-ray photoelectron spectroscopy (XPS) (Fig. 1d), which showed a clear Sb $3d_{3/2}$ peak at 539.5 eV. This peak position suggests that the Sb atoms substitute Zn atoms (Sb_{Zn})[18]. Sb distribution along the nanowires was also proved by Auger electron spectroscopy (AES), as shown in Supplementary Figs S5 and S6.

Lasing of the nanowires was first demonstrated using optical pumping. Figure 1e shows the lasing spectra at different pumping powers. Equidistant peaks with a separation of ~2.4 nm can be observed (solid arrows). At higher pumping powers, additional modes (indicated by dashed arrow) also begin to emerge as a result of the excitation of adjacent nanowires with slightly different lengths. The threshold power (P_{th}) was found to be ~180 kW cm^{-2} from a plot of the intensity as a function of pumping power (Fig. 1e, inset). The density of electron–hole pairs (n_p) produced by the optical pumping can be calculated as $n_p = I_{exc}\tau/h\omega l$ (ref. 19), where I_{exc} is the excitation power, τ is the spontaneous emission lifetime (τ varies[20] and is assumed to be 300 ps, ref. 21) and l is the diffusion length (~2 μm, ref. 22, from top excitation). The analysis gives an n_p of ~5.1×10^{17} cm^{-3} at threshold.

In Fig. 2a, the current–voltage (I–V) characteristics show a rectifying diode behaviour. However, the large reverse current is related to the formation of an indium tin oxide (ITO)/Sb-doped ZnO nanowire metal–semiconductor junction, which is in series with the ZnO p-n homojunction. The formation of the ZnO homojunction between the nanowires and film was investigated by electron-beam-induced current (EBIC) profiling[23,24]. To facilitate the EBIC experiment, silver paste was used to contact the top ends of the nanowires. Figure 2b shows the EBIC profile superimposed on a cross-sectional scanning electron microscopy (SEM) image. The EBIC signal forms a peak across the nanowire/film junction due to the drift of electron-beam generated electrons and holes under the influence of the built-in electric field, indicating the formation of a p-n junction. The second peak on the right side is

[1]Quantum Structures Laboratory, Department of Electrical Engineering, University of California at Riverside, Riverside, CA 92521 USA, [2]Laboratory of Advanced Materials, Department of Physics, Fudan University, Shanghai, 200433 China, [3]Department of Physics, University of Central Florida, Orlando, FL 32816 USA, [4]School of Physics and Optoelectronic Engineering, Dalian University of Technology, Dalian, 116024 China; †These authors contributed equally to this work. *e-mail: jianlin@ee.ucr.edu

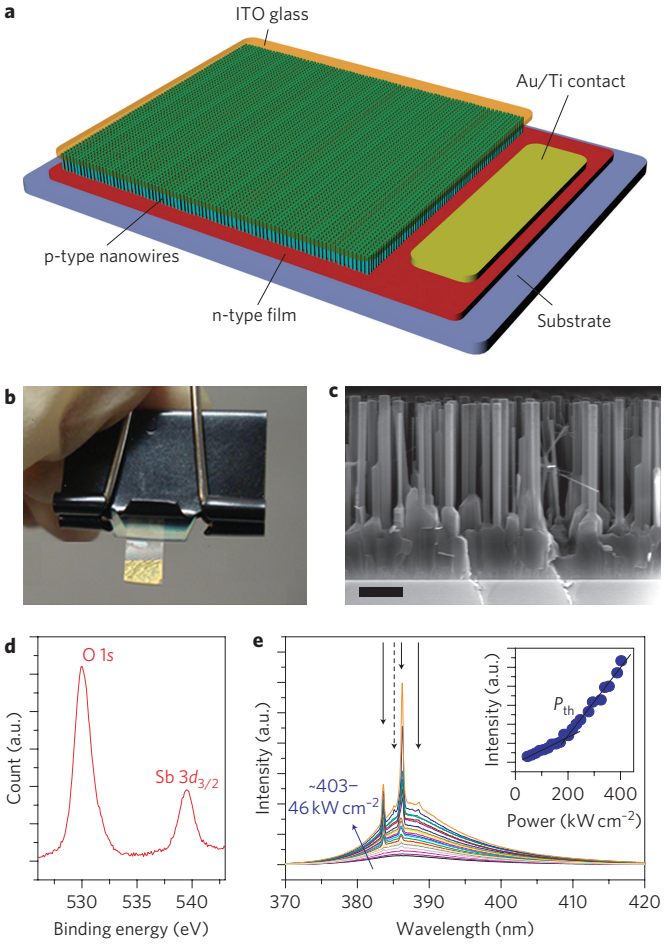

Figure 1 | Structure and material properties of the ZnO nanowire/film laser device. a, Schematic of the laser device, which consists of an n-type ZnO thin film on a *c*-sapphire substrate, p-type vertically aligned ZnO nanowires, ITO contact and Au/Ti contact. **b**, Photo-image of the device. **c**, Side-view SEM image of the device structure showing the ZnO thin film and nanowires. Scale bar, 1 μm. **d**, XPS spectrum of the Sb-doped ZnO nanowires array. **e**, Room-temperature optically pumped lasing spectra from 46 kW cm^{-2} to 403 kW cm^{-2} with average steps of ~20 kW cm^{-2}. Solid arrows denote equidistant lasing peaks, and a spacing of 2.4 nm is extracted. Inset: integrated spectra intensity as a function of pumping power density. Solid lines represent threshold P_{th} (~180 kW cm^{-2}).

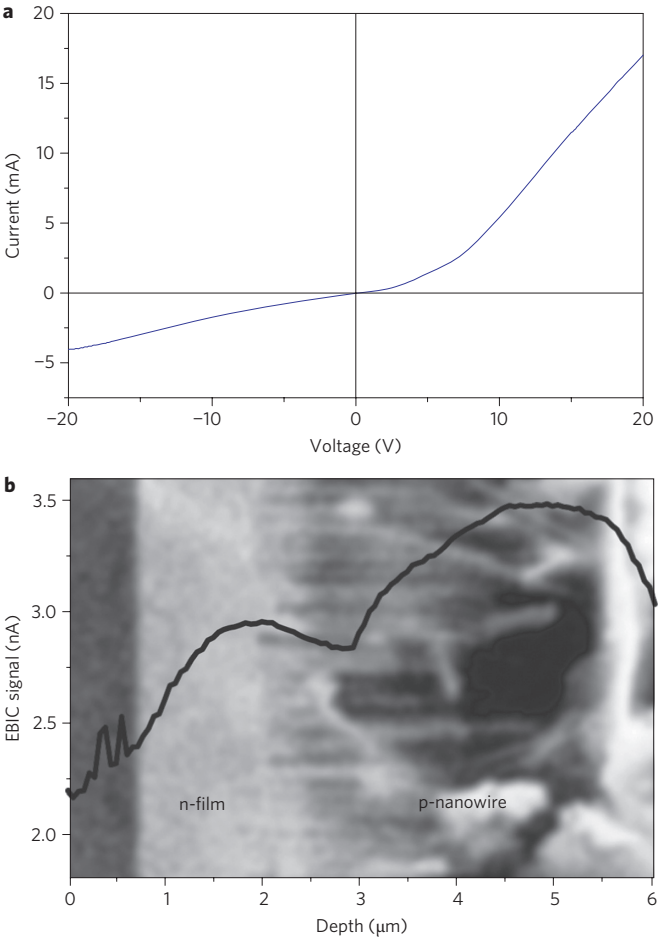

Figure 2 | *I–V* properties and evidence of the formation of a ZnO nanowire/film p-n junction. a, *I–V* characteristic of the ITO/ZnO nanowire/ZnO film laser device. Positive bias is applied on the ITO side. **b**, EBIC profile superimposed on the side-view SEM image of the cleaved device.

related to the additional non-equilibrium electron collection from the ZnO/ITO/silver paste contacts. The p-type conductivity of the ZnO nanowires can be demonstrated by field-effect measurement (Supplementary Figs S7 and S8). A hole concentration of 4.5×10^{17} to 2.5×10^{18} cm^{-3} is extracted, and the electrical properties are comparable to those of p-type ZnO nanogenerators[12]. Moreover, these carriers seem to be degenerate[25] (Supplementary Fig. S9), and can potentially give rise to efficient hole injection for lasing. In addition, low-temperature photoluminescence studies reveal acceptor-associated emission features in the Sb-doped ZnO nanowires (Supplementary Fig. S10).

Electroluminescence characterizations were performed to demonstrate the lasing action. Fig. 3a presents electroluminescence spectra under an injection current of between 20 mA and 70 mA. Under low injection currents (from 20 to 40 mA), only free-exciton spontaneous emissions centred at ~385 nm are observed. As the pump current reaches a threshold of ~50 mA, drastic sharp emissions with line-widths as narrow as 0.5 nm emerge from the single broad emission around 385 nm, which indicates that the gain is now large enough to enable the cavity mode to start lasing. A further increase in the injection current stimulates the onset of lasing in additional nanowires with slightly different lengths, resulting in an increase in the number of lasing peaks. A stable, quasi-equidistant pattern of lasing peaks can be extracted with reasonable wavelength deviation. The average spacing between modes ($\Delta\lambda$) is 2.52 nm for the selected peaks denoted by arrows in Fig. 3a, which is close to the spacing in optical pumping obtained from Fig. 1e (2.4 nm). Spacing $\Delta\lambda$ for a FP cavity is given by the expression $\Delta\lambda = \lambda^2[2L(n - \lambda(dn/d\lambda))]^{-1}$ (ref. 11), where $n = 2.5$ is the refractive index of ZnO and $dn/d\lambda = -0.015$ nm^{-1} denotes the dispersion relation for the refractive index. For a 4.2 μm cavity between the top end of the ZnO nanowire and the bottom ZnO film/sapphire interface (determined by SEM imaging), $\Delta\lambda$ is calculated to be 2.95 nm, which is in close agreement with the observed experimental values. Another device with a longer cavity length of 10 μm was fabricated, and the line spacing was also found to be consistent with the value calculated from the above formula (Supplementary Figs S11 and S12).

In addition to the spectral features, the far-field microscope images in Fig. 3b show direct evidence of nanowire FP-type lasing. A side view of a ZnO nanowire array can be seen in the centre of the first image. The illumination lamp was switched off and emission light was recorded for the biased device with excitation

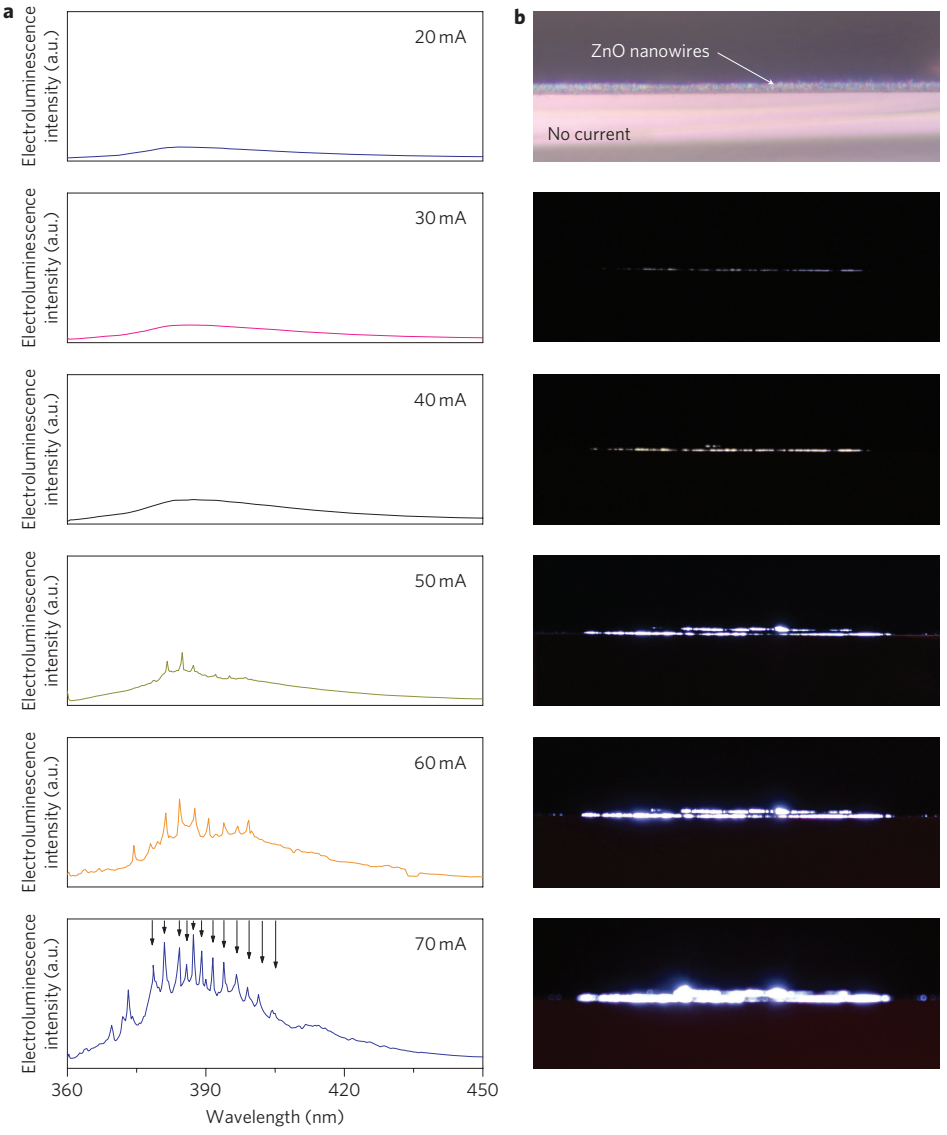

Figure 3 | Laser emission characterizations. a, Electroluminescence spectra of the laser device operated between 20 mA and 70 mA. Above 50 mA, lasing characteristics are clearly observed. Arrows in the 70 mA spectrum represent quasi-equidistant peaks. **b**, Side-view optical microscope images of the lasing device, corresponding to the electroluminescence spectra in **a**. The first image was taken with lamp illumination and without current injection.

currents from 30 mA to 70 mA. Under excitation with 30 mA, distinct light emission can be observed, which forms a stripe close to the bottom of the nanowires/thin film interface, indicating that electrically pumped light emission starts near the p-n junction active region rather than at the ITO/ZnO nanowire interface. With an increase in the injection current, light emerges from the top ends of the nanowires. As the pumping current increases to 60 or 70 mA, this behaviour becomes very striking, with bright light spot pairs at the two ends of the nanowires. This phenomenon comprises strong proof of longitudinal lasing modes in a waveguide that has been constantly observed in optically pumped nanowire lasing[3,11,26].

The integrated lasing spectrum intensity is plotted against injection current in Fig. 4a. The dashed line is a guide to the eye, showing an evident threshold current of ~48 mA. The gain/feedback mechanism of this nanowire/thin film FP laser is shown in Fig. 4b. It can be inferred that the gain length is determined by the minority carrier diffusion lengths in the p-type nanowire ($L_n \approx 2$ μm; ref. 22) and n-type ZnO film ($L_p \approx 200$ nm; ref. 27), as well as the width of the space charge region (<100 nm). The total gain length is therefore ~2.3 μm. In a FP laser, the threshold gain G_{th} is given as[26]

$$G_{th} = \frac{1}{2L}\ln\left(\frac{1}{R_1 \times R_2}\right)$$

where R_1 and R_2 are the reflectivities on the two ends of the cavity (0.04 for sapphire/ZnO and 0.09 for ZnO/ITO/glass), and L is the gain length. A calculated value of G_{th} gives $\sim 1.2 \times 10^4$ cm^{-1} for this laser. However, optically pumped lasing (Fig. 1e) needs a reduced G_{th} of $\sim 5.6 \times 10^3$ cm^{-1}, mainly due to the longer L (4.2 μm) and larger reflectivity at the ZnO/ITO/air interface (0.2). An excited carrier density of 5.1×10^{17} cm^{-3} was estimated at threshold for optically pumped lasing in the previous paragraph, so it is reasonable to assume that higher carrier densities, for example $>1.0 \times 10^{18}$ cm^{-3}, are needed in the electrically pumped case because of the larger G_{th}. These numbers are around or larger than the calculated Mott density of ZnO (ref. 19, 28) so electron–hole plasma (EHP) rather than an exciton–exciton interaction

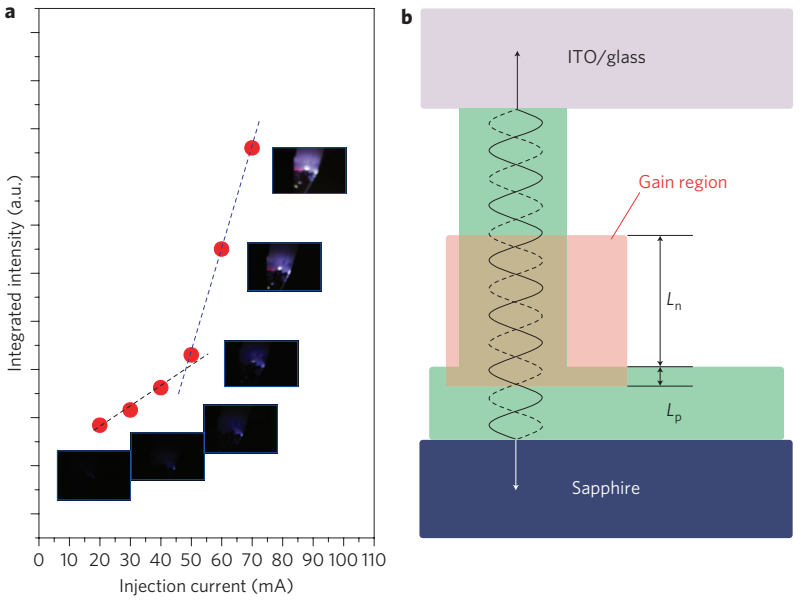

Figure 4 | Lasing threshold gain/feedback properties. a, Integrated spectrum intensity as a function of injection current. Dashed line is a guide to the eye. Inset: camera images corresponding to the emission pattern along the nanowire length direction at each injection current. **b**, Gain feedback diagram of the ZnO nanowire/thin-film laser cavity. The laser gain area (red) is defined by the diffusion length L_n and L_p.

may dominate the lasing process. Using $n_p = I_{th}\tau/eV_{gain}$ (ref. 19), where I_{th} is the threshold current and $V_{gain} = L \times S$ (S, nanowire cross-sectional area) is the volume of the gain region, threshold current in each lasing nanowire, I_{th}, is determined to be >39 μA. This is comparable with the threshold current of 200 μA measured in a CdS nanowire laser[11]. This situation can be readily achieved due to the fact that the initial current crowding effect will allow a handful of nanowires among those tightly connected with ITO/glass contacts to meet the threshold gain and lase, with a further increase in injection current causing more nanowires to lase. The laser diode is quite stable, and can produce FP-stimulated lasing with only slightly degraded output power even six and seven months after the first test (Supplementary Figs S13, S14 and S15).

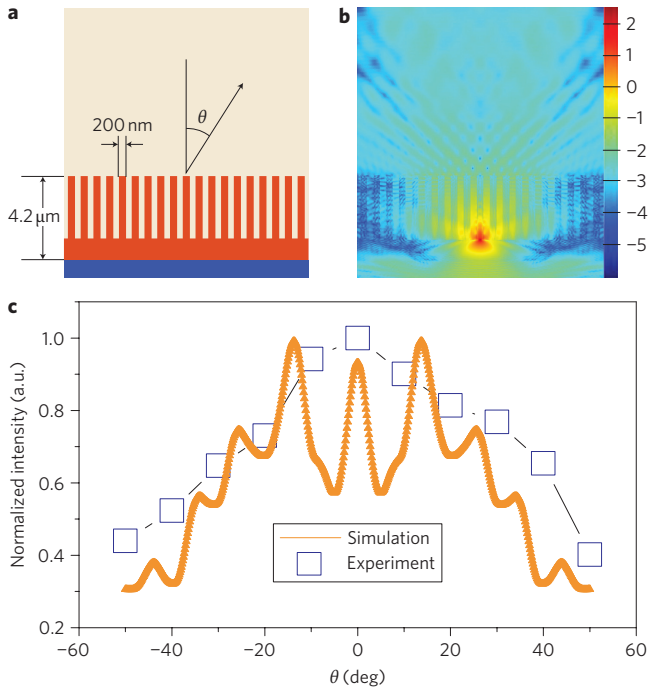

Figure 5 | Far-field pattern of light emission. a, Schematic of the FDTD simulation/measurement environment (area, 9 × 10 μm^2). **b**, Simulated spatial distribution of the light (385 nm) intensity. **c**, Angle distribution of the far-field emission patterns (the x-axis represents the emission angle θ with respect to the nanowire growth direction and the y-axis represents the normalized emission intensity). Orange curve, simulation results; blue squares, results from electroluminescence measurements when rotating the device with respect to the nanowire length direction.

Under injection currents corresponding to the red dots in Fig. 4, lasing images were taken from the nanowire length direction (Fig. 4, inset). Blue-purple light becomes significantly brighter as the pumping increases above threshold. The evolution of the spatial distribution of the emissions was studied by finite-difference time-domain (FDTD) simulations (see Methods). The simulation/measurement environment is schematically illustrated in Fig. 5a. The simulated spatial distribution of the emission is presented in Fig. 5b, and the far-field emission intensity as a function of angle with respect to the nanowire length direction in Fig. 5c. The results suggest that the nanowire laser device emits intense light close to the nanowire length direction, and the light spreads in a concentrated conic shape with angular oscillation. The simulated pattern (orange line) closely follows the results of previous nanowire laser studies[3,26,29,30]. The experimental far-field emission values (blue squares) in Fig. 5c are in close agreement with the simulated data of the far-field pattern, further proving the waveguide mode emission.

In conclusion, we have achieved the fabrication of electrically pumped ZnO nanowire diode lasers using p-type Sb-doped ZnO nanowires and n-type ZnO film. FP-type UV lasing was demonstrated at room temperature with good stability. Work on ZnO UV lasing may facilitate many potential applications. Future work is needed to further optimize laser performance. For example, the top contact with the p-type nanowire might be engineered to offer both good optical transparency and low electrical resistivity. Also, heterojunction nanowire diode structures may be used to achieve stronger power output.

Methods

ZnO thin film growth. The n-type ZnO film was grown on a 2-inch c-plane sapphire substrate using plasma-assisted MBE. Growth began with a 1 min growth of MgO to improve subsequent ZnO film quality, followed by a regular ZnO buffer layer growth at 550 °C for 8 min. The main ZnO film was then grown at

700 °C for 5 h, yielding a total film thickness of ~1,050 nm. The Zn effusion cell temperature was kept at 360 °C with a beam flux on the order of 1×10^{-7} torr. Oxygen plasma was generated by a radiofrequency system and the flow rate of oxygen was 5 s.c.c.m.

ZnO nanowire growth. The *c*-axis oriented ZnO thin film acted both as a seed layer for ZnO nanowire growth and also as an n-type component of the p-n junction light-emitting device. The ZnO/*c*-sapphire sample was subsequently transferred to a CVD furnace for vapour–solid growth of Sb-doped ZnO nanowires. The sample was partially covered during nanowire growth to expose the ZnO film for n-type contact deposition.

The ZnO nanowires were grown using a quartz tube furnace system (Thermal Scientific Inc.). Zinc powder (99.999% Sigma Aldrich) in a glass bottle was placed in the centre of the quartz tube. Sb powder (99.99% Sigma Aldrich) was put into an open glass boat. The boat was placed ~5 cm upstream of the zinc source. The ZnO film sample was kept 10 cm away from the zinc source on the downstream side. A flow of 1,000 s.c.c.m. nitrogen was passed continuously through the furnace. The sources and sample were then heated to 650 °C at a ramp rate of 30 °C min^{-1}. Once the desired temperature was reached, 200 s.c.c.m. of a mixture of argon/oxygen (99.5:0.5) was introduced to the quartz tube for ZnO nanowire growth. Growth was maintained for 15 min.

Device fabrication. For the n-type contact, a Au/Ti (100 nm/10 nm) contact was deposited on the n-type ZnO films (the n-contact area was intentionally covered during nanowire growth). For the top ITO contact, following ZnO nanowire formation, polymethyl methacrylate (PMMA) was spun onto the sample to separate the bottom ZnO film and subsequent ITO top contact. The spin rate was 2,000 r.p.m. for 30 s, and this process was repeated five times. After drying, the sample was placed in a d.c. magnetron sputtering system. The ITO target (99.99%) was acquired from Sigma Aldrich. The growth was carried out at room temperature and the pressure maintained at 1×10^{-2} torr. The sputtering power and time were 180 W and 10 min, respectively. The ITO glass slides (~15–25 Ω/sq) for the reliable current feedthrough were acquired from Sigma Aldrich. The fabricated device had an area of $\sim 5 \times 10$ mm^2.

EBIC measurement. EBIC profile measurements were conducted on the ZnO nanowire/ZnO film cross-sectional structure by cleaving the sample. Measurement was carried out in a Philips XL30 SEM under a 30 kV electron-beam accelerating voltage. EBIC signal line scans were recorded using homemade software. A Stanford Research System low-noise current amplifier and a Keithley 2000 digital multimeter were used as the digitizer.

Photo- and electroluminesence measurements. The system consisted of an Oriel monochromator and a lock-in amplifier with a chopper. A 325 nm He–Cd laser was used as the excitation source. A photomultiplier tube was used to detect device light emission, which emanated from the ITO/glass electrode from the nanowires. The scan step for the photo- and electroluminescence was 0.3 nm. An external HP E3630A d.c. power supply was used to input current for electroluminescence measurement. To record the far-field lasing pattern, a Nikon Eclipse L200 microscope was equipped with a Sony DXC 970 charge-coupled device (CCD) camera. For the optically pumped lasing demonstration, the system was built by using a UV enhanced objective (×40) and Princeton Instrument monochromator equipped with a silicon CCD. The laser excitation source was a Nd:YAG pulse laser with an output wavelength of 355 nm (3 ns pulse).

Scanning AES measurement. A PHI 700 Scanning Auger Nanoprobe system was used for Sb-dopant profile distribution characterization. A reference sample grown under the same conditions was used for characterization.

FDTD simulation. FDTD solution 6.5 (Lumerical Inc.) was used for simulation. The pumping source was a point transverse electric wave (380 nm to ~400 nm) source located between the ZnO nanowire (centre one) and the ZnO film, which corresponds to the p-n junction active area. The diameter and length of the nanowire were 200 nm and 3.2 μm, respectively. The distance between nanowires was 400 nm. The thickness of the ZnO film was 1.05 μm. A frequency-domain power monitor was used to record the emission profile over the simulation region.

Received 30 March 2011; accepted 24 May 2011; published online 3 July 2011

References

1. Yan, R., Gargas, D. & Yang, P. Nanowire photonics. *Nature Photon.* **3,** 569–576 (2009).
2. Huang, M. H. *et al.* Room-temperature ultraviolet nanowire nanolasers. *Science* **292,** 1897–1899 (2001).
3. Vugt, L. K. V., Rühle, S. & Vanmaekelbergh, D. Phase-correlated nondirectional laser emission from the end facets of a ZnO nanowire. *Nano Lett.* **6,** 2707–2711 (2006).
4. Zhou, H. *et al.* Ordered, uniform-sized ZnO nanolasers arrays. *Appl. Phys. Lett.* **91,** 181112 (2007).
5. Kwok, W. M. *et al.* Influence of annealing on stimulated emission in ZnO nanorods. *Appl. Phys. Lett.* **89,** 183112 (2006).
6. Gargast, D. *et al.* Whispering gallery mode lasing from ZnO hexagonal nanodisks. *ACS Nano* **4,** 3270–3276 (2010).
7. Ma, X. Y. *et al.* Room temperature electrically pumped ultraviolet random lasing from ZnO nanorod arrays on Si. *Opt. Express* **17,** 14426–14433 (2009).
8. Liang, H. K., Yu, S. F. & Yang, H. Y. Directional and controllable edge-emitting ZnO ultraviolet random laser diodes. *Appl. Phys. Lett.* **96,** 101116 (2010).
9. Zhu, H. *et al.* Low threshold electrically pumped random lasers. *Adv. Mater.* **22,** 1877–1881 (2010).
10. Chu, S., Olmedo, M., Kong, J. Y., Yang, Z. & Liu, J. L. Electrically pumped ultraviolet ZnO laser diode. *Appl. Phys. Lett.* **93,** 181106 (2008).
11. Duan, X. F., Huang, Y., Agarwal, R. & Lieber, C. M. Single-nanowire electrically driven lasers. *Nature* **421,** 241–245 (2003).
12. Lu, M. P. *et al.* Piezoelectric nanogenerator using *p*-type ZnO nanowire arrays. *Nano Lett.* **9,** 1223–1227 (2009).
13. Tsukazaki, A. *et al.* Repeated temperature modulation epitaxy for *p*-type doping and light-emitting diode based on ZnO. *Nature Mater.* **4,** 42–46 (2005).
14. Chen, M. *et al.* Near UV LEDs made with *in situ* doped *p-n* homojunction ZnO nanowire arrays. *Nano Lett.* **10,** 4387–4393 (2010).
15. Wang, G. *et al.* ZnO homojunction photodiodes based on Sb-doped p-type nanowire array and n-type film for ultraviolet detection. *Appl. Phys. Lett.* **98,** 041107 (2011).
16. Greence, L. E. *et al.* General route to vertical ZnO nanowire arrays using texured ZnO seeds. *Nano Lett.* **5,** 1231–1236 (2005).
17. Wu, Y. W., Yeh, C. C. & Ting, J. M. Effects of seed layer characteristics on the synthesis of ZnO nanowires, *J. Am. Ceram. Soc.* **92,** 2718–2723 (2009).
18. Izquierdo, R., Sacher, E. & Yelon, A. X-ray photoelectron spectra of antimony oxides. *Appl. Surf. Sci.* **40,** 175–177 (1989).
19. Klingshirn, C., Hauschild, R., Fallert, J. & Kalt, H. Room-temperature stimulated emission of ZnO: alternatives to excitonic lasing. *Phys. Rev. B* **75,** 115203 (2007).
20. Hauschild, R., Priller, H., Decker, M., Kalt, H. & Klingshirn, C. The exciton polariton model and the diffusion of excitons in ZnO analyzed by time-dependent photoluminescence spectroscopy. *Phys. Status Solidi C* **3,** 980–983 (2006).
21. Reynolds, D. C. *et al.* Time-resolved photoluminescence lifetime measurements of the Γ_5 and Γ_6 free excitons in ZnO. *J. Appl. Phys.* **88,** 2152–2153 (2000).
22. Lopatiuk-Tirpak, O. *et al.* Studies of minority carrier diffusion length increase in p-type ZnO:Sb. *J. Appl. Phys.* **100,** 086101 (2006).
23. Hoffmann, S. *et al.* Axial *p-n* junctions realized in silicon nanowires by ion implantation. *Nano Lett.* **9,** 1341–1344 (2009).
24. Chernyak, L. *et al.* Electron beam induced current profiling of ZnO *p-n* homojunctions. *Appl. Phys. Lett.* **92,** 102106 (2008).
25. Salfi, J., Philipose, U., Aouba, S., Nair, S. V. & Ruda, H. E. Electron transport in degenerate Mn-doped ZnO nanowires. *Appl. Phys. Lett.* **90,** 032104 (2007).
26. Johnson, J. C., Yan, H. Q., Yang, P. D. & Saykally, R. J. Optical cavity effects in ZnO nanowire lasers and waveguides. *J. Phys. Chem. B* **107,** 8816–8828 (2003).
27. Soudi, A., Dhakal, P. & Gu, Y. Diameter dependence of the minority carrier diffusion length in individual ZnO nanowires. *Appl. Phys. Lett.* **96,** 253115 (2010).
28. Versteegh, M. A. M., Kuis, T., Stoof, H. T. C. & Dijkhuis, J. I. Ultrafast screening and carrier dynamics in ZnO: theory and experiment. Preprint at http://arXiv.org/abs/1012.3600 (2010).
29. Friedler, I. *et al.* Solid state single photon sources: the nanowire antenna. *Opt. Express* **17,** 2095–2110 (2009).
30. Zimmler, M. A., Bao, J., Capasso, F., Muller, S. & Ronning, C. Laser action in nanowires: observation of the transition from amplified spontaneous emission to laser oscillation. *Appl. Phys. Lett.* **93,** 051101 (2008).

Acknowledgements

The authors would like to thank K.N. Bozhilov for assistance in TEM imaging, Z.H. Chen for guidance in optical pumping measurements and D. Paul for AES measurement and analysis. The work on the ZnO device was in part supported by Army Research Office Young Investigator Program (grant no. W911NF-08-1-0432) and by the National Science Foundation (grant no. ECCS-0900978). The work on p-type ZnO was supported by the Department of Energy (DE-FG02-08ER46520).

Author contributions

S.C., G.W. and J.L. conceived and designed the experiments. S.C., G.W. and J.Z. carried out the experiments. Y.L. and L.C. performed and analysed the EBIC experiment. W.Z. performed the lasing measurement by optical pumping. S.C. and J.K. carried out theoretical simulations. J.R. and L.L. contributed material analysis. S.C., G.W. and J.L. co-wrote the paper. J.L. supervised the project.

Additional information

The authors declare no competing financial interests. Supplementary information accompanies this paper at www.nature.com/naturenanotechnology. Reprints and permission information is available online at http://www.nature.com/reprints. Correspondence and requests for materials should be addressed to J.L.